Journal of Advanced Marine Engineering and Technology, Vol. 48, No. 5, pp. 268~276, 2024
J. Advanced Marine Engineering and Technology (JAMET)
https://doi.org/10.5916/jamet.2024.48.5.268

ISSN 2234-7925 (Print)
ISSN 2765-4796 (Online)
Original Paper

Experimental investigation of coaxial flow-assisted propane diffusion flames for soot emission reduction

Jong Hyun Park[1] · Suhyeon Kim[2] · Min-Gyu Jeon[3] · Sung Hwan Yoon[†]

(Received October 15, 2024 ; Revised October 18, 2024 ; Accepted October 29, 2024)

Abstract: Hydrocarbon-based fuels, such as propane (LPG), emit pollutants like soot during combustion, which negatively affect human health and the environment. Propane, with lower carbon emissions than diesel and gasoline, is a promising low-carbon bridge fuel. The study investigates nitrogen-diluted propane diffusion flames, specifically examining flame structures by introducing coaxial flow aspiration, where the oxidizer flow is set in the opposite direction to the fuel injection velocity at the nozzle. A total of 72 different mixtures were tested, varying fuel dilution ratios, aspiration flow rates, and nozzle injection velocities. The results identified five distinct flame regimes—Natural Convection-Dominated Flame (Regime I), Inside-Out Soot Flame (Regime II), Mushroom-shaped Flame (Regime III), Cylindrical Flame (Regime IV), and Inhibited Natural Convection Flame (Regime V). As aspiration flow rates increased, the flame structure transitioned from a typical diffusion flame in Regime I to a microgravity-like diffusion-dominated blue flame in Regime V under strong negative coaxial aspiration. Notably, coaxial flow aspiration resulted in soot particle reductions of up to 86%. The study also characterized the normalized flame length and Froude number under the coaxial aspiration conditions, and based on this analysis, proposed a predictive model for flame length as a function of aspiration flow velocity.

Keywords: Propane, Diffusion flame, Coaxial flow, Exhaust gas, Aspiration flow

1. Introduction

In recent years, global efforts to reduce greenhouse gas (GHG) emissions have intensified, with major international organizations like the European Union (EU) and the U.S. Environmental Protection Agency (EPA) tightening emission standards across various industries such as automotive, aviation, and shipping **[1]**. Among these, the shipping industry, which accounts for approximately 3% of global GHG emissions, faces particularly stringent regulations. In 2023, the International Maritime Organization (IMO) introduced revised GHG strategies to further address these emissions. The main goal of these strategies is to reduce GHG emissions by 20–30% by 2030, 70–80% by 2040, and to achieve net-zero emissions by 2050 **[2]**.

The IMO's strategy promotes a shift to low- and zero-carbon marine fuels, such as hydrogen, ammonia, and biofuels, while addressing technical and economic challenges. The shipping sector is also implementing emission pricing mechanisms and marine fuel standards to accelerate the adoption of cleaner technologies and encourage investments in sustainable shipping infrastructure **[2]**. However, conventional fossil fuels like heavy fuel oil (HFO) and marine gas/diesel oil (MGO/MDO) still dominate, and their combustion results in significant emissions of pollutants, including carbon dioxide (CO_2), particulate matter (PM), and soot (black carbon). Soot is formed due to incomplete combustion of fuel, often existing as polycyclic aromatic hydrocarbons (PAHs) **[3]**. PAHs are formed when aromatic rings collide and bind during combustion, and the HACA (H–Abstraction–C_2H_2–Addition) mechanism plays a crucial role in soot formation **[4]**. The soot particles formed through this process grow via surface growth and agglomeration, and soot that escapes oxidation

† Corresponding Author (ORCID: https://orcid.org/0000-0001-5794-3286): Associate Professor, Department of Marine System Engineering, Korea Maritime & Ocean University, 727, Taejong-ro, Yeongdo-gu, Busan 49112, Korea, E-mail: shy@kmou.ac.kr, Tel: +51-410-4261

1 M. S. candidate, Department of green and smart ship equipment, Korea Maritime & Ocean University, E-mail: tech@eit-one.com, Tel: +82-51-973-2030

2 Ph. D. Candidate, Department of Marine System Engineering, Korea Maritime & Ocean University, E-mail: edwsqa8624@g.kmou.ac.kr, Tel: +82-51-410-4261

3 Assistant Professor, Department of Mechanical System Engineering, Republic of Korea Naval Academy, E-mail: mgjeon@navy.ac.kr, Tel: +82-55-907-5335

in the flame region is emitted as black carbon. These particles can accumulate in the respiratory system, leading to long-term respiratory and cardiovascular diseases. Furthermore, studies have shown that long-term exposure to particulate matter can affect cognitive and mental functions, emphasizing the risks posed by air pollutants **[5]**.

As the demand for a low-carbon society grows, various industries, including shipping, automotive, and industrial machinery, are developing and adopting eco-friendly technologies to reduce GHG emissions. Technologies such as after-treatment devices, improved combustion efficiency, and green fuel transitions are being introduced, but achieving complete zero emissions remains a significant technical and economic challenge **[6]**. While next-generation technologies like hydrogen fuel cells and electric propulsion systems are essential for realizing zero emissions, they face substantial barriers to immediate commercialization. As a result, there is increasing interest in bridge fuels that can serve as transitional solutions between conventional fuels and fully green alternatives. Fuels like liquefied natural gas (LNG), methanol, and liquefied petroleum gas (LPG) are seen as useful options for improving existing fuel systems due to their relatively lower carbon emissions. Specifically, LPG emits less soot and particulate matter compared to gasoline or diesel, can utilize existing infrastructure, and has lower liquefied storage costs.

LPG has traditionally been used for domestic, commercial, portable cooking, and heating purposes, but its demand in South Korea is increasing for applications such as city gas co-combustion, LNG-LPG mixed power generation, and LPG gas heat pumps. Market analyses project that the global LPG market will grow from approximately $88.5 billion in 2023 to around $122.6 billion by 2032, with a compound annual growth rate (CAGR) of about 4.1% **[7]**. In the shipping sector, LPG's low vapor pressure and favorable liquefaction temperature help reduce fuel storage costs and efficiently utilize existing infrastructure. As a result, interest in the development of LPG-specific engines is growing, and orders for LPG-powered ships are on the rise. In June 2023, the IMO approved international guidelines for LPG-powered ships, accelerating the adoption of LPG in the shipbuilding and maritime industries **[8]**.

Despite LPG's relatively lower CO_2 emissions compared to HFO, MGO, and MDO, soot emissions remain a significant issue. Previous studies have shown that increasing external air flow in a coaxial burner delays soot formation, reducing peak soot concentration **[9]**. Furthermore, increasing the primary air by 10% of the fuel's stoichiometric air requirement can result in a 70% reduction in maximum soot concentration. Generally, soot formation occurs at the cooler outer edges of the flame due to incomplete combustion **[10]**. Carbon particles formed through pyrolysis grow into soot particles through surface growth, agglomeration, and oxidation. Choi *et al.* categorized soot formation into non-sooting flames, where complete oxidation occurs within the flame zone, and sooting flames, where incomplete soot is emitted **[11]**. Therefore, in diffusion flames, the scalar dissipation rate, which is influenced by the intensity of oxidizer inflow, is a crucial factor in determining soot concentration **[12][13]**.

Numerous researchers have explored strategies to reduce soot in non-premixed flames. Kalvakala *et al.* **[14][15]** investigated ethylene, propane, and propylene counterflow diffusion flames under atmospheric and elevated pressures, demonstrating that both hydrodynamic effects and flame structure modifications play crucial roles in reducing PAHs and soot, with hydrodynamic effects becoming more significant at higher oxygen levels. Similarly, Lou *et al.* **[16]** experimentally showed that soot-free flames can be achieved by raising the stoichiometric mixture fraction (Z_{st}) through a combination of fuel dilution with recycled flue gas (CO_2) and oxygen enrichment in the oxidizing stream. These studies highlight the flexibility of oxy-flames, offering the ability to control flame temperature and fuel concentration while independently managing soot formation.

While existing research has predominantly focused on suppressing soot formation, the present study introduces a novel approach that considers soot management from a carbon capture perspective. This work aims to not only inhibit soot formation but also capture it effectively, contributing to enhanced combustion efficiency and reduced environmental impact. By applying a coaxial aspiration flow configuration, we assess the potential of this approach to simultaneously control soot emissions and capture soot particles, providing valuable insights into advanced clean combustion technologies. Therefore, this study investigates the dynamic flame behavior of nitrogen-diluted propane diffusion flames with the introduction of coaxial aspiration flow, evaluating the potential for capturing soot emissions. The flame behavior is analyzed under five distinct flame regimes, categorized based on aspiration intensity and nozzle exit velocity. Additionally, a predictive model for flame length as a function of aspiration flow velocity is proposed.

2. Experimental method

2.1 Experimental Method

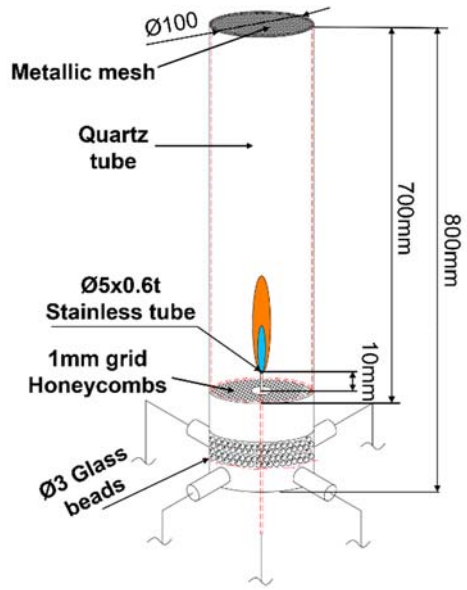

Figure 1: Co-axial burner detail setup

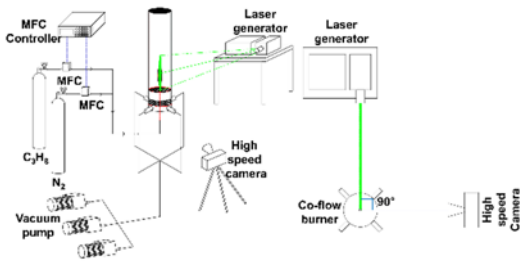

Figure 2: Experimental setup diagram

The experimental setup, as depicted in **Figures 1** and **2**, was designed to investigate the dynamic behavior of diffusion flames in a coaxial burner, based on the well-known "Santoro burner" configuration. The burner assembly included a stainless steel tube with an outer diameter of 5 mm and an inner diameter of 3.8 mm, centrally positioned within a burner body made of stainless steel, with a total diameter of 100 mm. Four ports were installed at 90° intervals around the lower section of the burner to facilitate the coaxial application of exhaust flow.

To ensure uniform exhaust flow, glass beads and a ceramic honeycomb structure were placed inside the burner's lower section, which evenly distributed the exhaust gases. The stainless steel nozzle was set to protrude 10 mm above the ceramic honeycomb, a height that was experimentally validated for producing the most stable diffusion flame. To minimize the effects of external air disturbances, a quartz tube with a diameter of 100 mm and a height of 700 mm was placed above the burner. A fine metal mesh was installed at the top of the quartz tube to ensure uniform oxygen flow over the fuel.

During baseline flame conditions, without the operation of vacuum pumps, rapid oxygen depletion inside the quartz tube resulted in flame extinction. To address this, an acrylic chamber with sufficient internal volume and open top and bottom was used in cases where the baseline flame was employed, ensuring stable airflow. This setup helped induce uniform airflow, thereby stabilizing the flame.

To control the flow rates of the gases accurately, mass flow controllers were used, and calibration was performed using a precision calibrator to ensure accurate propane-nitrogen mixture flow rates. Urethane tubing with an outer diameter of 6 mm and an inner diameter of 4 mm was used for the fuel injection lines, with a separation distance of over 1 meter to ensure sufficient dilution. The exhaust lines, connected to vacuum pumps, were constructed using urethane tubes with an outer diameter of 12 mm and an inner diameter of 8 mm, ensuring adequate flow.

Three vacuum pumps were employed, each providing a aspiration velocity of −20 cm/s. Preliminary experiments using Mie scattering-based Particle Image Velocimetry (PIV) were conducted to confirm the exhaust flow rate before final testing.

The flame's dynamic behavior was captured using a high-speed camera (Photron, Fastcam SA3), operating at a resolution of 768×1024 pixels and 250 fps (frames per second). These high-speed images were subsequently used for velocity field measurements, utilizing Particle Image Velocimetry (PIV). The acquired data were analyzed using an open-source MATLAB-based code, ensuring accuracy in velocity field estimations.

2.2 Experimental Conditions

The fuel mixtures used in this experiment were classified into four categories based on the dilution ratio of propane to nitrogen, as shown in **Table 1**. The selected ratios, in decreasing order of propane concentration, were 1:0, 0.5:0.5, 0.2:0.8, and 0.15:0.85. For mixtures with a propane concentration below 0.15, flame extinction occurred across most flow rates, making further experimentation impossible under these conditions. In total, 72 experiments were conducted under various conditions, and the resulting flame structures were classified according to their distinct visual characteristics.

The aspiration flow velocity produced by the vacuum pumps was varied based on the number of pumps in operation.

Table 1: Experimental conditions

Mixture	X_f (Fuel mole fraction)		U_{co} [cm/s]	U_f [cm/s]
	C_3H_8	N_2		
1	1.00	0.00	0 −40 −60	20–60
2	0.50	0.50		20–120
3	0.20	0.80		20–180
4	0.15	0.85		20–120

Specifically, the velocities were set at 0 cm/s (baseline flame), −40 cm/s (using two pumps), and −60 cm/s (using three pumps). When only one pump was operated, the exhaust velocity was too low to significantly affect the flame's flow dynamics, and thus this condition was excluded from further analysis.

The nozzle flow velocity of the gas mixture through the nozzle began at a minimum of 20 cm/s and was increased incrementally by 20 cm/s. Conditions that resulted in either natural flame extinction or lifted flames were excluded from the analysis. For pure propane flames, the experiment was conducted safely by observing the diffusion flame only up to two-thirds of the total burner height, limiting the flow velocities between 20 cm/s and 60 cm/s.

Lastly, the highest temperatures at the stoichiometric plane for each fuel mixture were calculated using the PREMIX code in CHEMKIN II package **[17]**. The calculated maximum temperatures were as follows: 2010.5 K for Mixture 1, 1944.9 K for Mixture 2, 1782.9 K for Mixture 3, and 1706.9 K for Mixture 4.

3. Result and Discussion

3.1 Analysis of Flame Structure

In this study, a comprehensive flame analysis was conducted across 72 experiments by adjusting key parameters, such as the propane-to-nitrogen dilution ratio, the fuel nozzle injection velocity, and the coaxial aspiration flow. Based on these variables, the flames were classified into five distinct regimes, and the characteristics of each regime were thoroughly analyzed.

Figure 3 illustrates the various flame structures observed in the study:

- **Regime I** (Natural Convection-Dominated Flame): This regime was observed when there was no coaxial aspiration. The flame exhibited a typical diffusion flame structure, where the fuel interacted with ambient oxygen, forming a clear velocity profile as predicted by jet similarity solutions. The average flame height

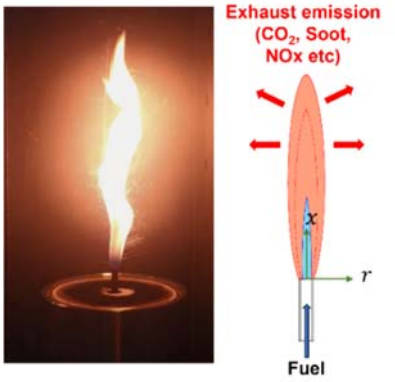

(a) Regime I

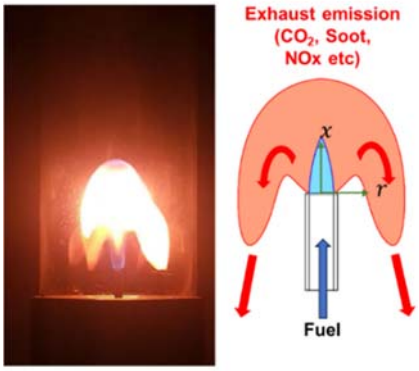

(b) Regime II

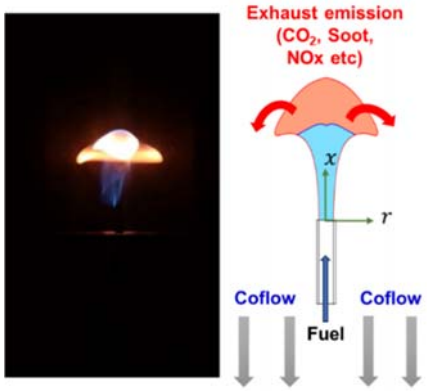

(c) Regime III

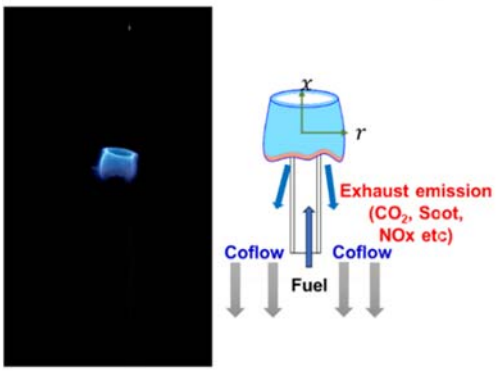

(d) Regime IV

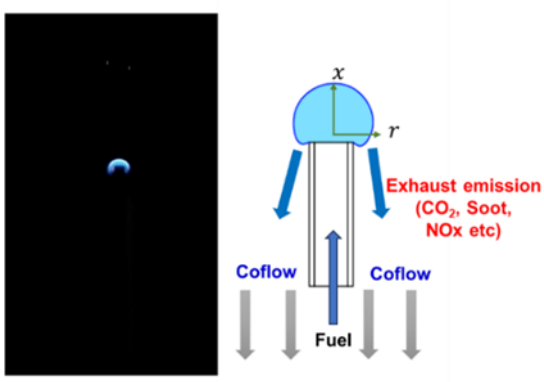

(e) Regime V

Figure 3: Flame formation structure

was measured at 20.9 cm, with a maximum height of 30.2 cm.

- **Regime II** (Inside-Out Soot Flame): With a coaxial aspiration velocity of −40 cm/s, and a fuel dilution ratio of 0.5 with a nozzle exit velocity of 100 cm/s, the flame showed soot-rich regions pulled downward by the aspiration flow. The average flame height was 9 cm, and the maximum height reached 11.7 cm.
- **Regime III** (Mushroom-shaped Flame): Under conditions where the fuel dilution ratio was 0.2, the nozzle exit velocity was 60 cm/s, and the coaxial aspiration velocity was −40 cm/s, the soot-rich region of the flame took on a ring-like shape around the flame. The average flame height was 4.7 cm, and the maximum height was 6.2 cm.
- **Regime IV** (Cylindrical Flame): This regime was observed at a fuel dilution ratio of 0.15, a nozzle exit velocity of 60 cm/s, and a coaxial aspiration velocity of −60 cm/s. The flame tip had a distinct crown-like shape with a hollow center. The soot emission was minimal, and the flame was very stable, with an average height of 1.6 cm and a maximum of 2.7 cm.
- **Regime V** (Inhibited Natural Convection Flame): At a fuel dilution ratio of 0.15, a nozzle exit velocity of 20 cm/s, and a coaxial aspiration velocity of −40 cm/s, a small, low-velocity blue flame tip resembling a microgravity flame was noted, with minimal soot emissions. The average flame height was 1.1 cm, and the maximum height was 1.2 cm, showing remarkable stability.

In this study, the coaxial diffusion flames observed across 72 experiments were categorized into five regimes (Regime I to

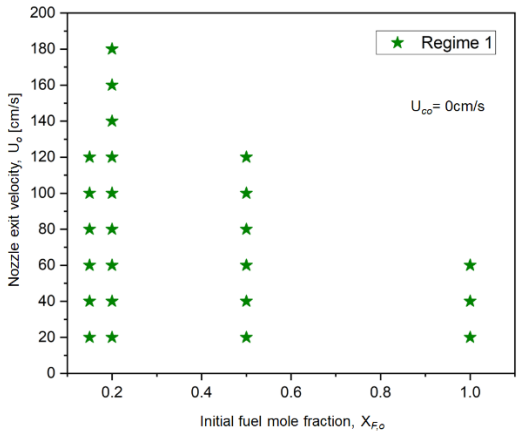

(a)

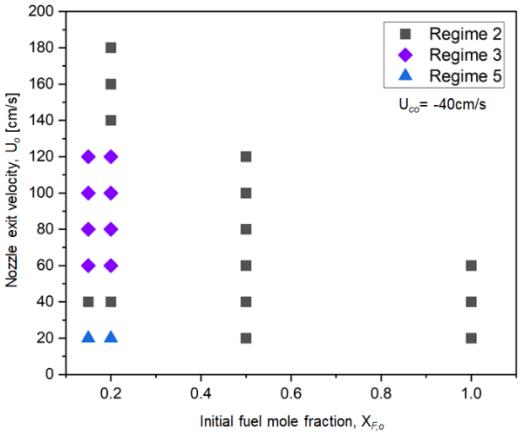

(b)

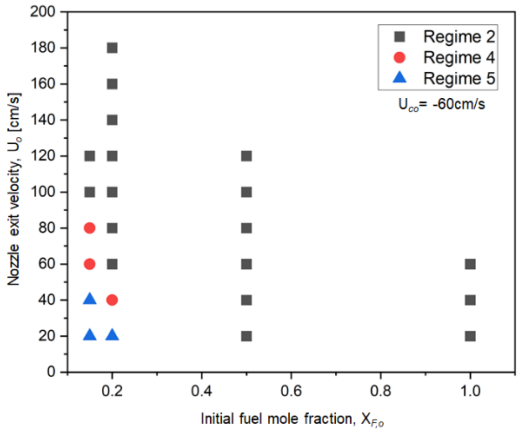

(c)

Figure 4: Flame stability maps illustrating the relationship between initial fuel mole fraction and nozzle exit velocity under varying aspiration velocities: (a) U_{co} = 0cm/s, (b) U_{co} = −40cm/s, and (c) U_{co} = −60cm/s

Regime V), and their distributions were mapped as stability maps (**Figs. 4a**, **4b**, and **4c**). These maps depict the relationship between the initial fuel mole fraction and nozzle exit velocity under different aspiration conditions. Each stability map provides

insight into how variations in aspiration velocity impact flame structure and emission characteristics.

Figure 4a presents the stability map under U_{co} = 0 cm/s (no aspiration flow). In all 24 experimental trials, the absence of aspiration resulted in baseline diffusion flames (Regime I), where the jet similarity solution predicted the typical diffusion flame behavior. No significant soot reduction was observed in these conditions.

Figure 4b depicts the stability map under $U_{co} = -40$ cm/s, with two vacuum pumps in operation. At $X_{F,O} \geq 0.5$, Regime II flames emerged, characterized by soot emission being pulled downward by the coaxial aspiration flow. The intense downward movement of these emissions formed the inside-out soot flame structure. At lower $X_{F,O}$ (≤ 0.2) and low nozzle exit velocity (20 cm/s), the flames resembled microgravity flames (Regime V) with minimal soot emissions. As the nozzle velocity increased to 40 cm/s, soot regions started to reappear and sink downward, resulting in Regime II re-emerging. At 60 cm/s, the interaction between the jet momentum and coaxial aspiration formed ring-shaped flames (Regime III) around the flame core.

Figure 4c shows the stability map under $U_{co} = -60$ cm/s, with three vacuum pumps in operation. Similar to the $U_{co} = -40$ cm/s condition, fuel-rich flames ($X_{F,O} \geq 0.5$) showed Regime II characteristics, with emissions being drawn downwards. At leaner fuel conditions ($X_{F,O} \leq 0.2$) and nozzle velocities of 20 ~ 40 cm/s, small, stable blue flames (Regime V) were observed at the nozzle tip, closely resembling microgravity flames. When the nozzle velocity was further increased, the flame tip split and moved downward, forming crown-like flames (Regime IV). Even with the slight emergence of red luminous regions, the flames were quickly drawn into the aspiration flow, limiting visible soot formation. As the nozzle velocity continued to increase, the flame transitioned back into Regime II, with increased flame area and emissions interacting with the aspiration flow and being pulled downwards.

In summary, when no coaxial aspiration flow was applied, a typical diffusion flame structure was consistently observed across all conditions (Regime I). However, as fuel output increased, leading to higher soot emission, the flame transitioned into Regime II. With increasing aspiration velocity, the flame structure progressively evolved through Regime II to Regime V, demonstrating clear changes in flame structure driven by the coaxial flow conditions.

3.2 Characterization of Flame Dynamics and Soot Volume Fraction

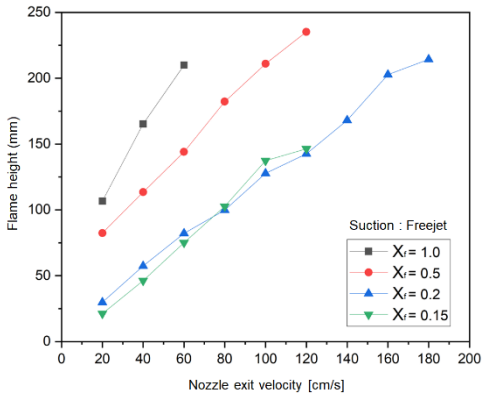

(a) U_{co} = 0 cm/s

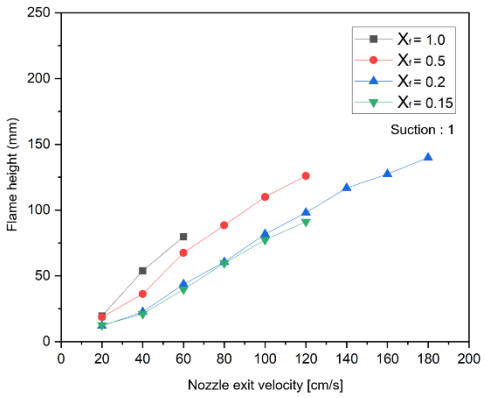

(b) $U_{co} = -40$ cm/s

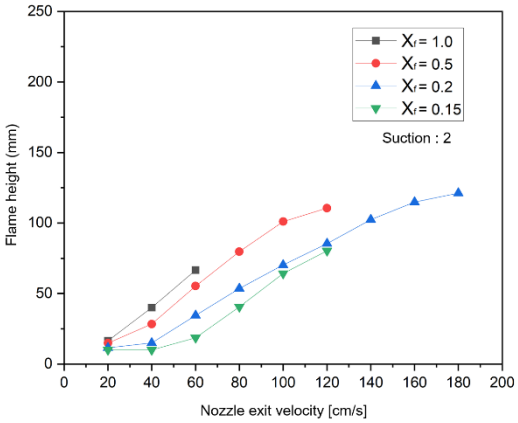

(c) $U_{co} = -60$ cm/s

Figure 5: Average flame height with various aspiration flow velocities

To evaluate the effect of aspiration flow velocity on flame height, the experimental results are illustrated in **Figure 5**. In **Figure 5a**, which depicts the case of U_{co} = 0 cm/s, the flame length increases with rising nozzle exit velocity. This extension can be attributed to the increased inflow of reactants per unit time, which promotes a larger reaction zone as the fuel interacts

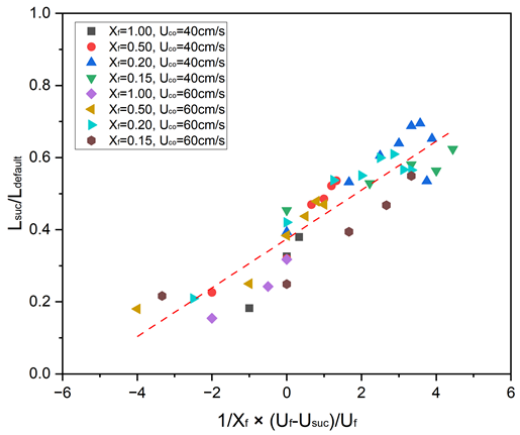

Figure 6: Relationship between normalized flame length and dimensionless parameter

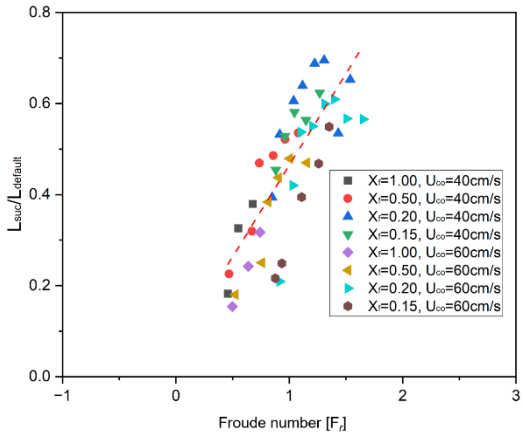

Figure 7: Characterization of flame ratio and non dimensional Froude number

with the oxidizer more extensively. Furthermore, the data shows a reduction in flame length as the fuel mole fraction decreases at a fixed nozzle exit velocity. This trend suggests that, as the concentration of nitrogen (acting as an inert diluent) rises, the chemical reaction rate decreases significantly. The reduced reactivity is likely due to volumetric heat losses introduced by the increased presence of inert gas, which does not participate in combustion. Notably, these general trends remain consistent even as aspiration flow velocities are increased.

In the experimental setup, the aspiration velocities were adjusted to three levels (0 cm/s, −40 cm/s, and −60 cm/s). As illustrated in the figure, the overall trend demonstrates a progressive decrease in the average flame height with increasing aspiration flow velocity. This reduction suggests that the rise in aspiration velocity causes the stagnation plane at the flame tip to move closer to the nozzle. Consequently, the flame length decreases, likely due to the enhanced influx of oxidizer into the reaction zone, which suppresses soot formation. Moreover, the intensified aspiration flow appears to effectively facilitate the removal of CO_2 and soot emissions from the flame, further promoting cleaner combustion.

Figure 6 illustrates the relationship between the normalized flame length ($L_{suc}/L_{default}$) and a dimensionless parameter expressed as $(U_f - U_{co})/(X_f \times U_f)$. In this study, L_{suc} represents the flame length under coaxial aspiration flow conditions, while $L_{default}$ refers to the default flame length without any aspiration flow applied. U_f denotes the nozzle exit velocity, indicating the speed at which fuel is injected through the nozzle, and U_{co} defines the aspiration flow velocity, representing the coaxial flow speed in the opposite direction to fuel injection. Finally, X_f refers to the mole fraction of the fuel, specifying the proportion of fuel within the overall mixture.

As illustrated in the figure, a linear relationship is observed between the normalized flame length and the dimensionless parameter. Notably, the normalized flame length decreases as the fuel mole fraction increases. This indicates that flames with longer lengths—where more soot is typically generated—exhibit a greater soot reduction effect when coaxial aspiration flow is applied. Furthermore, when the aspiration flow velocity is relatively higher than the nozzle exit velocity, the flame length shortens, resulting in a similarly enhanced soot reduction effect. This linear relationship is mathematically expressed in **Equation (1)**:

$$L_{suc}/L_{default} = 0.068\frac{(U_f - U_{co})}{X_f.U_f} + 0.37 \quad (1)$$

To quantitatively assess the relationship between inertial and gravitational forces in the flame flow field, the dimensionless parameter known as the Froude number was adopted and used to characterize the normalized flame length, as shown in **Figure 7**. The Froude number is defined as follows **Equation (2)**:

$$Fr = \frac{U_f}{\sqrt{gL}} \quad (2)$$

where g is the gravitational acceleration (9.81 m/s²) and L is the flame height.

A Froude number greater than 1 indicates that inertial forces dominate over gravitational forces, while a Froude number less than 1 suggests that gravitational effects are more influential. The analysis revealed that as the nozzle exit velocity decreased, both the Froude number and flame height also decreased. This

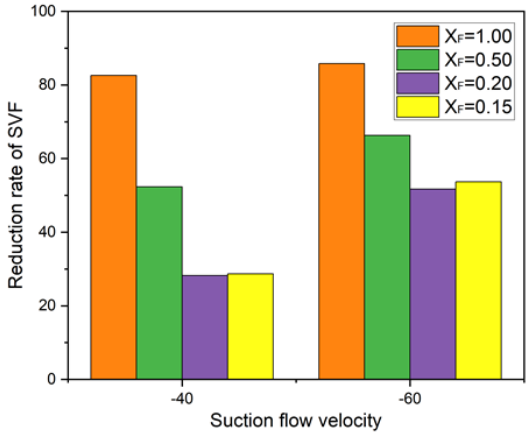

Figure 8: Reduction rate of soot volume fraction

transition reflects a flow field increasingly governed by gravitational forces due to the strong aspiration flow velocity. Consequently, soot formation within the flame was mitigated under these conditions. In contrast, when the nozzle exit velocity increased, the reduction in flame height became less noticeable, and the increased inertial force maintained the Froude number above 1. Additionally, the results demonstrated a linear increase in normalized flame length with increasing Froude number, indicating a proportional relationship between these two variables.

Additionally, as shown in **Figure 8**, soot volume fractions were calculated to measure the reduction in soot emissions under varying aspiration flow velocities and flame formation variables. To estimate the soot volume fraction, we adopted a method based on RGB analysis aligned with blackbody radiation principles, counting pixels corresponding to the visible light spectrum range associated with soot. While this approach may introduce some potential error, it remains an effective method for quantitative evaluation. Furthermore, to enhance accuracy, we calculated average values from images captured over a 10-second period. This averaging process mitigates the impact of flame fluctuation, offering a more reliable assessment than a single-frame inverse Abel transformation.

The reduction in soot volume, visualized in **Figure 8**, was analyzed under different fuel dilution ratios and aspiration velocities. The study found that higher fuel dilution ratios resulted in more significant reductions in soot volume, with a fuel dilution ratio of 1.00 and a aspiration flow velocity of −60 cm/s achieving a maximum soot reduction rate of 86%.

In conclusion, increasing aspiration velocity led to reductions in both flame height and soot volume, illustrating the impact of varying aspiration flow velocities and fuel dilution ratios on flame structure and emission characteristics.

4. Conclusion

This study presents an experimental investigation into the dynamic behavior of nitrogen-diluted propane diffusion flames under coaxial aspiration flow, with a focus on reducing soot emission. The results demonstrated that the flame structure and emission characteristics are significantly influenced by the fuel dilution ratio, nozzle injection velocity, and coflow aspiration velocity. Specifically, five distinct flame regimes were identified, each exhibiting unique flame shapes and emission profiles depending on the intensity of the coaxial aspiration.

Key findings of the study include the following:

1. **Effective Emission Control**: The application of coaxial aspiration flow successfully controlled emissions by reducing both flame height and soot particle concentration. This effect was most pronounced in Regime V, where the flame resembled a microgravity flame with minimal soot emissions.
2. **Significant Soot Reduction**: Under strong negative coaxial flow conditions (up to −60 cm/s), a maximum soot reduction rate of 86% was achieved. This highlights the efficiency of coaxial aspiration in minimizing soot formation during propane combustion, making it a promising technique for clean combustion systems.
3. **Predictive Model for Flame Length**: A linear relationship between flame length and key combustion parameters was established, allowing for accurate predictions of flame behavior based on fuel dilution ratio, injection velocity, and aspiration flow rate. This provides valuable insights for optimizing burner designs in industrial applications.
4. **Optimization of Fuel Combustion**: By systematically adjusting the fuel composition and coflow conditions, the study demonstrates the potential to optimize propane combustion efficiency while reducing environmental pollutants, contributing to the development of more sustainable combustion technologies.

Acknowledgement

This study was conducted with support of the research fund from the academic research project of the Republic of Korea Naval Academy's Ocean Research Institute in 2024.

Author Contributions

Conceptualization, J. H. Park and S. H. Yoon; Methodology, J.

H. Park and S. Kim; Software, J. H. Park and M. G. Jeon; Validation, J. H. Park and S. H. Yoon; Formal Analysis, J. H. Park and S. Kim; Investigation, J. H. Park and M. G. Jeon; Resources, First Author; Data Curation, J. H. Park; Writing—Original Draft Preparation, J. H. Park and S. Kim; Writing—Review & Editing, M. G. Jeon and S. H. Yoon; Visualization, J. H. Park; Supervision, M. G. Jeon and S. H. Yoon; Project Administration, M. G. Jeon and S. H. Yoon; Funding Acquisition, S. H. Yoon.

References

[1] J. Y. Moon, S. H. Oh, Y. S. Park, S. H. Lee, and E. M. Kim, "Increased International Greenhouse Gas Reduction Targets and South Korea's Response Measures," Korea Institute for International Economic Policy, pp. 1-17, 2020.

[2] IMO, IMO's Work to cut GHG Emission from Ships, IMO Media Centre, 2023.

[3] W. Ramsay, E. Fridell, and M. Michan, "Maritime energy transition: Future fuels and future emissions," Journal of Marine Science and Application, pp. 681-692, 2023.

[4] J. Appel, H. Bockhorn, and M. Frenklach "Kinetic modeling of soot formation with detailed chemistry and physics: Laminar premixed flames of C_2 hydrocarbons," Combustion and Flame, vol. 121, pp. 122-136, 2000.

[5] C. K. Law, Combustion Physics, Cambridge University Press, pp. 178-196, 2006.

[6] D. H. Kim, Y.-K. Lee, and D. W. Kwon, "Trends of cleaner alternative marine fuels and exhaust emission abatement technology for carbon neutrality," KIC News, vol. 25, no. 2, pp. 8-27, 2022.

[7] Precedence Research Propane Market Report, https://www.precedenceresearch.com/propane-market, Accessed May 5, 2024.

[8] IMO, International Maritime Organization MSC.1/Circ.1394/Rev.2 : Generic Guidelines For Developing IMO Goal Based Standards.

[9] H. A. K. Shahad and Y. K. A. Mohammed, "Investigation of soot formation and temperature field in laminar diffusion flames of LPG-air mixture," Energy Conversion and Management, vol. 41, pp. 1897-1916, 2000.

[10] S. Zhu, J. Yu, L. Chen, R. Zhu, X. Wu, and K. Cen, "Effects of blending methane, propane and propylene on soot evolution in ethylene diffusion flames based on optical diagnostics," Fuel, vol. 334, pp. 1-14, 2023.

[11] I.-C. Choi, J.-B. Lee, J.-H. Hwang, "Characterization of soot particles generated in non sooting and sooting normal diffusion flames," Transactions of the Korean Society of Mechanical Engineers B, vol. 24, no. 7, pp. 984-993, 2000.

[12] S. H. Yoon, J. Park, O. B. Kwon, and D.-S. Bae, "Study of Characteristic of Self-Excitation in Lifted Laminar Free-Jet Propane Flames Diluted with Nitrogen," Transactions of the Korean Society of Mechanical Engineers B, vol. 34, pp. 399-408, 2010.

[13] S. H. Yoon, J. Park, O. B. Kwon, J. H. Yoon, S. I. Keel, J. S. Kim, and D.-S. Bae, "Experimental study on self-excitations in nitrogen-diluted laminar lifted butane flames," Fuel, vol. 91, pp. 51-60, 2012.

[14] K. C. Kalvakala, V. R. Katta, and S. K. Aggarwal, "Effects of oxygen-enrichment and fuel unsaturation on soot and NOx emissions in ethylene, propane, and propene flames," Combustion and Flame, vol. 187, pp. 217-229, 2018.

[15] K. C. Kalvakala and S. K. Aggarwal, "Polycyclic aromatic hydrocarbons and soot emissions in oxygenated ethylene diffusion flames at elevated pressures," Journal of Engineering for Gas Turbines and Power, vol. 141, no. 7, 071022, 2019.

[16] L. Chun, C. Xiaobing, Y. Weijie, T. Yanfei, and B. M. Kumfer, "Effect of stoichiometric mixture fraction on soot fraction and emission spectra with application to oxy-combustion," Proceedings of the Combustion Institute, vol. 37, no. 4, pp. 4571-4578, 2019.

[17] R. J. Kee, F. M. Rupley, and J. A. Miller, "CHEMKIN-II: A Fortran Chemical Kinetics Package for Analysis of Gas Phase Chemical Kinetics," Sandia National Laboratories: Albuquerque, NM, SAND 89-8009B, 1989.